Journal of Computational Applied Mechanics 2024, 55(3): 519-537

DOI: 10.22059/jcamech.2024.372417.968

RESEARCH PAPER

A novel quasi-3D refined HSDT for static bending analysis of porous functionally graded Plates

Rachid Slimani [a], Abderrahmane Menasria [b,c], Mohamed Ali Rachedi [b,c], Mourad Chitour [c], Salah Refrafi [c], Ali Alselami Nimer [d,*], Abdelhakim Bouhadra [b,c], Belgacem Mamen [b,c]

[a] *University of Tamanghasset, Faculty of Sciences & Technology, Sciences & Technology Department, BP 10034, Sersouf Tamanghasset 11000, Algeria*

[b] *Materials and Hydrology Laboratory, University of Sidi Bel Abbes, Faculty of Technology, Civil Engineering Department, BP 89, Sidi Bel Abbes 22000, Algeria*

[c] *University of Khenchela, Faculty of Sciences and Technology, Civil Engineering Department, BP 1252 Road of Batna Khenchela, Khenchela 40000, Algeria*

[d] *Civil Engineering Department, College of Engineering, Jazan University, Saudi Arabia*

Abstract

In this paper a quasi-three-dimensional (3D) refined using a novel higher-order shear deformation theory is developed to examine the static bending with two different type porosity distribution of porous for advanced composite plates such as functionally graded plates. In this present theory, the number of unknowns and governing equations is reduced, takes into account the thickness stretching effect into transverse displacement, bending and shear, using a new shape function. The used plate theory approach satisfies the zero traction boundary conditions on the surfaces of the plate without using shear correction factor and the transverse shear strain and shear stress have a parabolic distribution across the thickness of the plates. The virtual work principle is used to obtain the equilibrium equations. An analytical approach based on the Navier solution is employed to obtain the solution for static bending of simply supported FGM plates. The proposed theory shows a good agreement for static bending of FGM plates with other literature results has been instituted of advanced composite plates. Numerical results are presented to show the effect of the material distribution, the power-law FG plates, the geometrical parameters and the porosity on the deflections and stresses of FG plates.

Keywords: Higher-order shear deformation theory; FG plate; P-FGM; E-FGM; Bending; Porosity; The virtual work principle; Navier solution.

1. Introduction

Recent attention has been paid to a new category of composite materials called materials (FGM). Following the lightest advantageous features with high strength/weight and rigidity/weight ratios

* Corresponding author. Tel.: ; *E-mail address:*

have been used successfully in the aeronautical industry, civil engineering, nuclear engineering and other engineering applications and to be used in high temperature condition, contrary with traditional composite material. In general, FGM is created from a mixture of metal and ceramic. Many researchers have devoted their time to understanding the mechanical behaviour and mechanism of FGMs to provide an optimum profile for designers, where they have been captivated to investigate the bending behaviors, buckling, free vibration and dynamic and behaviors of FGM beams, plates, and shells.

Therefore, because of the exotic properties of FGM, many researchers were captivated of bending behaviours for different solicitations, static, free vibrations and buckling behaviors of FGM beams, plates, and shells [1, 2]. According to the literature, FGM plate analysis can be studied using various theories such as classical plate theory (CPT) [3, 4], the first-order shear deformation theory (FSDT) [5, 6], higher-order shear deformation theory (HSDT) [28-35], the quasi-3D theory and Carrera unified formulation (CUF) [7, 8]. To determine the spatial variation of material properties in functionally graduated materials and structures, mathematical laws such as exponential law [9], sigmoid law [10] and power law [11] are used.

According to the literature, some work using a refined shear deformation plate theory RSDT to determine the behaviour of plates in FGM has been published. Merazi et al. [12] studied of the neutral surface position for static analysis of FGM plate using a trigonometric RSDT shear deformation plate theory. Reddy and Reddy [13] used a RSDT by dividing the transverse deflection into bending and shear components to see their contributions to the total transverse displacement. Benachour et al. [14] investigated a four variable refined plate theory for free vibrations of functionally graded plates with arbitrary gradient. Do et al. [15] examined the deflection, in-plane normal, and shear stresses of sinusoidally loaded FGM rectangular plates with four simply supported edges. Moreover, many articles are published concerning the analysis of FGM structures based on RSDT which involves only four unknown functions for flexion response, buckling response, thermo-mechanical bending and free vibration of simply supported FGM sandwich plate [16-21].

In the open literature, some studies about the effect of porosity in the FGM structures have been published. Merdaci et al. [22] studied the bending behaviour of FG plates with porosities that allow the plate to be perfectly porous and homogenous or to have a form of perfect homogeneity shape depending over the values of the density fraction of voids (porosity) or graded factors. Sidda Reddya et al. [13] established the influence of thickness stretching needs to be considered to analyze the bending behavior of FG porous plates, using a novel higher order Quasi-3D theory to the bending response of FGPs with different forms of porosities considering the transverse extensibility along the thickness direction. Khorshidvand et al. [23] studied static bending and mechanical buckling analyses of FGP plates based on a refined plate theory and the set of the governing equations are derived using minimum potential energy. Rad et al. [24] presented the static response of porous and multidirectional heterogenous structures based on developed gradient elastic foundations. Additional researchers are restricted their attention to vibration and buckling [25-29] or the buckling [1, 30-32] of many porous structures. Al-Furjan et al. [41] examined how waves move through a unique micro-sandwich beam with three distinct layers: an auxetic honeycomb core, a piezoelectric top layer, and a bottom layer that gradually changes its properties in two directions. The study analyzed how several factors, including material properties, geometric features, and specific characteristics of the bottom layer, influence the wave behavior. The findings indicated that a modified theory significantly increases the predicted wave speed compared to the traditional approach. Additionally, larger elements in the auxetic honeycomb core lead to faster wave propagation. Al-Furjan et al. [42] explored how

waves move through the wings of tiny flying machines (micro air vehicles) using a novel approach based on mathematical modeling. The study introduces a new design concept that utilizes special materials in the wings to improve their rigidity and control how waves propagate within them. Various factors affecting wave behavior, like the size of the MAV, specific materials used, and the presence of a magnetic field have been considered. Advanced mathematical techniques have been used to analyze and predict important wave characteristics in these unique wings. The results showed that applying a magnetic field significantly increases the wave speed within the wings.

The objective of this article is to present the bending behavior of FG plates having porosities. The plate may be either perfectly porous homogeneous or has a perfect homogeneity shape depending on the values of the volume fraction of voids (porosity) or of the graded factors. The plate is assumed isotropic at any point within the plate, with its Young's modulus varying across its thickness in accord with a power law in terms of the volume fractions of the plate constituents while the Poisson's ratio remains constant. The present theory satisfies equilibrium conditions at the plate's top and bottom faces without using shear correction factors. A Navier solution is used to obtain closed-form solutions for simply supported FG plates. Several important aspects, i.e. aspect ratios, thickness ratios, exponent graded factor as well as porosity volume fraction, which affect deflections and stresses, are investigated.

2. Material Properties of FGM Plates with different porosity distributions

Material composition is varying along z direction with the FG index k. The mechanical properties of the FG plate such as Young's modulus 'E', Poisson's ratio 'υ', shear modulus 'G' change as the material composition change. In this study, FGM plates with the power-law function (P-FGM) and exponential function (E-FGM) as shown in Figure 1 were considered.

For a P-FGM plate, the volume of ceramic is obtained using the following formula:

$$V(z)=\left(\frac{1}{2}+\frac{z}{h}\right)^{k} \tag{1}$$

in which k is the power-law index and h is the thickness of the plate. The material properties of a P-FGM can be determined as:

$$P(z)=P_2+(P_1-P_2)V(z) \tag{2}$$

The material properties of E-FGM can be determined as:

$$P(z)=P_2 e^{B(z+\frac{h}{2})} \quad \text{with} \quad B=\frac{1}{h}\ln\left(\frac{E_c}{E_m}\right) \tag{3}$$

The porosity is considered to be of two different types: even (type-I) and uneven (type-II) distribution of pores. The porosity volume fraction, which defines the density of the pores, is β (β<< 1). The modified rule of mixture for even (type-I) and uneven (type-II) is proposed as Shafiei et al. [13], Simsek. [14], Wattanasakulpong, and Chaikittiratana. [15]. For even porosity (type-I):

$$P(z)=P_2+(P_1-P_2)V-\frac{\beta}{2}(P_1+P_2) \tag{4}$$

For uneven (type-II):

$$P(z) = P_2 + (P_1 - P_2)V - \frac{\beta}{2}(P_1 + P_2)\left(1 - \frac{2|z|}{h}\right) \tag{5}$$

Where P is the effective material property. P1 and P2 are the properties of the upper and lower faces of plate respectively.

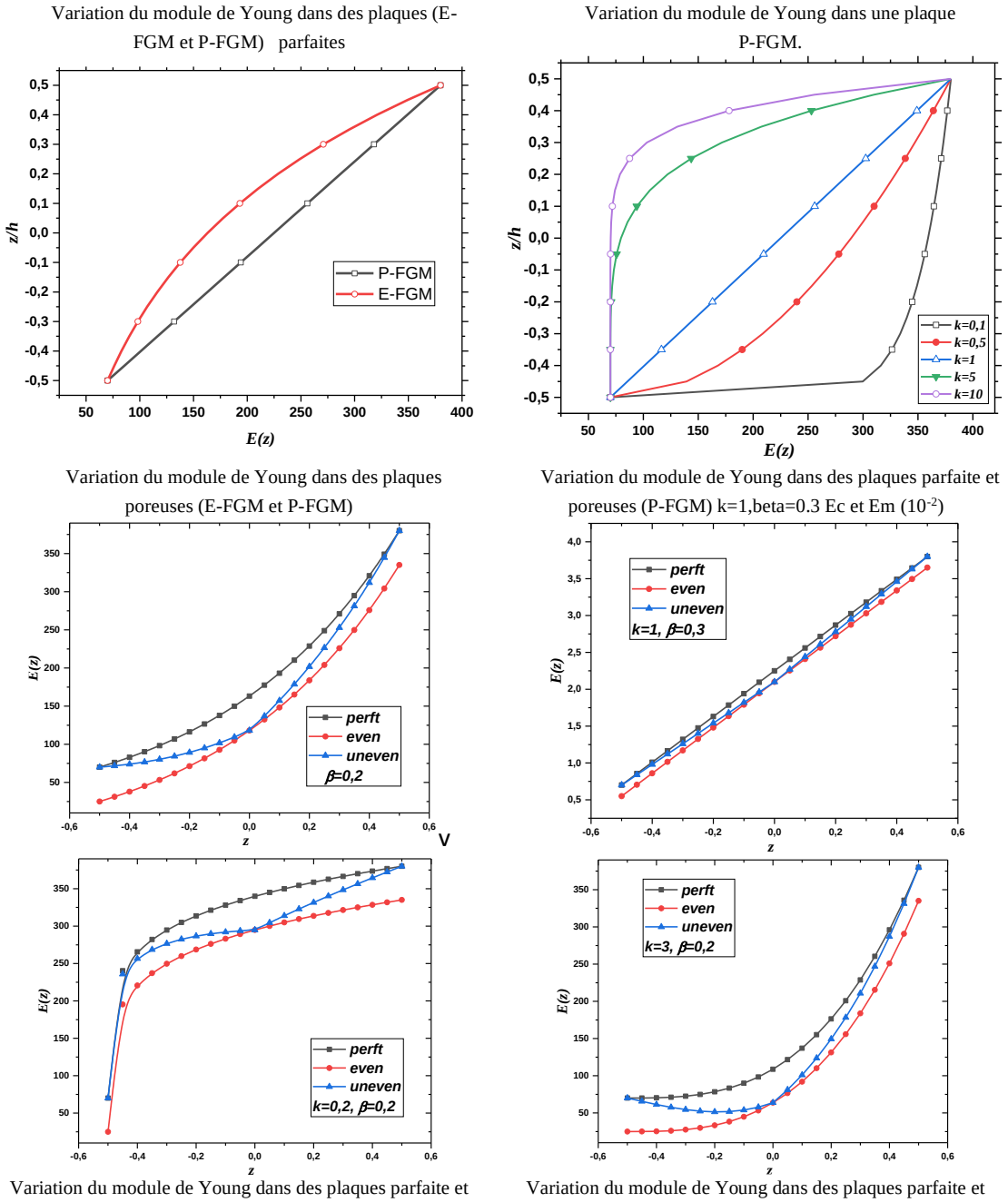

Fig 1: Young's modulus variation for different power laws

3. Kinematics

The FGM plate studied is of uniform thickness, length (a), width (b) and thickness (h). The upper and lower surfaces of the plate are at z =h/2 and z=-h/2, and the edges of the plate are parallel to the x and y axes.

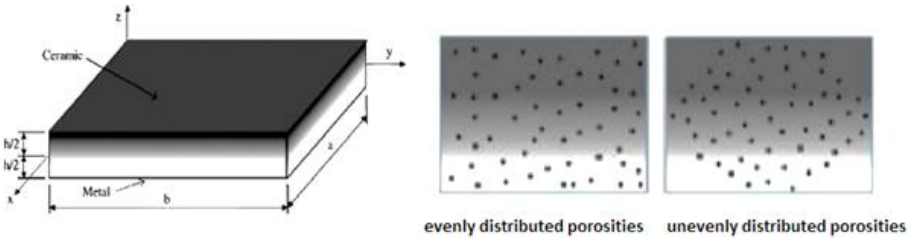

Fig 2 : Geometry and coordinates of the FG porous plate.

A quasi-3D refined HSDT assumptions are used and simplified to reduce the number of unknown variables. The current displacement fields takes into account the thickness stretching effect into transverse displacement, can be written as follows:

$$\begin{aligned} u(x,y,z) &= u_0(x,y) - z\frac{\partial w_b}{\partial x} + f(z)\frac{\partial w_s}{\partial x} \\ v(x,y,z) &= v_0(x,y) - z\frac{\partial w_b}{\partial y} + f(z)\frac{\partial w_s}{\partial y} \\ w(x,y,z) &= w_b(x,y) + g(z)w_s(x,y) \end{aligned} \tag{6}$$

In the present study, the new shape function $f(z)$ is proposed as follows:

$$\begin{aligned} f(z) &= \frac{5}{4}z - \frac{5}{3}\frac{z^3}{h^2} \\ g(z) &= r\frac{df(z)}{dz} \quad \text{and} \quad r = \frac{2}{15} \end{aligned} \tag{7}$$

Where $u_0(x,y)$, $v_0(x,y)$, $w_b(x,y)$ and $w_s(x,y)$ are the four unknown displacement functions of the middle surface of the plate. The kinematic relations can be obtained as follows:

$$\begin{Bmatrix} \varepsilon_x \\ \varepsilon_y \\ \gamma_{xy} \end{Bmatrix} = \begin{Bmatrix} \varepsilon_x^0 \\ \varepsilon_y^0 \\ \gamma_{xy}^0 \end{Bmatrix} + z\begin{Bmatrix} k_x^b \\ k_y^b \\ k_{xy}^b \end{Bmatrix} + f(z)\begin{Bmatrix} k_x^s \\ k_y^s \\ k_{xy}^s \end{Bmatrix}, \quad \varepsilon_z = g'(z)\varepsilon_z^0 \qquad \begin{Bmatrix} \gamma_{yz} \\ \gamma_{xz} \end{Bmatrix} = f'(z)\begin{Bmatrix} \gamma_{yz}^0 \\ \gamma_{xz}^0 \end{Bmatrix} + g(z)\begin{Bmatrix} \gamma_{yz}^0 \\ \gamma_{xz}^0 \end{Bmatrix} \tag{8}$$

$$\begin{Bmatrix} \varepsilon_x^0 \\ \varepsilon_y^0 \\ \gamma_{xy}^0 \end{Bmatrix} = \begin{Bmatrix} \dfrac{\partial u_0}{\partial x} \\ \dfrac{\partial v_0}{\partial y} \\ \dfrac{\partial u_0}{\partial y} + \dfrac{\partial v_0}{\partial x} \end{Bmatrix}, \quad \begin{Bmatrix} k_x^b \\ k_y^b \\ k_{xy}^b \end{Bmatrix} = \begin{Bmatrix} -\dfrac{\partial^2 w_b}{\partial x^2} \\ -\dfrac{\partial^2 w_b}{\partial y^2} \\ -2\dfrac{\partial^2 w_b}{\partial x \partial y} \end{Bmatrix}, \quad \begin{Bmatrix} k_x^s \\ k_y^s \\ k_{xy}^s \end{Bmatrix} = \begin{Bmatrix} \dfrac{\partial^2 w_s}{\partial x^2} \\ \dfrac{\partial^2 w_s}{\partial y^2} \\ 2\dfrac{\partial^2 w_s}{\partial x \partial y} \end{Bmatrix} \qquad \begin{Bmatrix} \gamma_{yz}^0 \\ \gamma_{xz}^0 \end{Bmatrix} = \begin{Bmatrix} \dfrac{\partial w_s}{\partial y} \\ \dfrac{\partial w_s}{\partial x} \end{Bmatrix}, \quad \varepsilon_z^0 = w_s \tag{9}$$

4. Constitutive relations

For elastic and isotropic FGMs, the constitutive relationships can be expressed as follows:

$$\begin{Bmatrix}\sigma_x\\ \sigma_y\\ \sigma_z\\ \tau_{yz}\\ \tau_{xz}\\ \tau_{xy}\end{Bmatrix}=\begin{bmatrix}C_{11} & C_{12} & C_{13} & 0 & 0 & 0\\ C_{12} & C_{22} & C_{23} & 0 & 0 & 0\\ C_{13} & C_{23} & C_{33} & 0 & 0 & 0\\ 0 & 0 & 0 & C_{44} & & \\ 0 & 0 & 0 & & C_{55} & \\ 0 & 0 & 0 & & & C_{66}\end{bmatrix}\begin{Bmatrix}\varepsilon_x\\ \varepsilon_y\\ \varepsilon_z\\ \gamma_{xy}\\ \gamma_{yz}\\ \gamma_{xz}\end{Bmatrix} \tag{10}$$

Where (σ_x , σ_y , σ_z , τ_{xy} , τ_{yz} , τ_{xz}) and (ε_x , ε_y , ε_z , γ_{xy} , γ_{yz} , γ_{xz}) are the components of the stress set deformations, respectively. The coefficients (Cij) are given by:

$$\begin{aligned}C_{11}&=C_{22}=C_{33}=\frac{E(z)(1-\nu)}{(1-2\nu)(1+\nu)}\\ C_{12}&=C_{13}=C_{23}=\frac{\nu E(z)}{(1-2\nu)(1+\nu)}\\ C_{44}&=C_{55}=C_{66}=\frac{E(z)}{2(1+\nu)}\end{aligned} \tag{11}$$

5. Equilibrium equations

Considering the static version of the principle of virtual work, the variation of strain energy of the plate is calculated by:

$$\int\int_A[\sigma_x\delta\varepsilon_x+\sigma_y\delta\varepsilon_y+\sigma_z\delta\varepsilon_z+\tau_{xy}\delta\gamma_{xy}+\tau_{xz}\delta\gamma_{xz}+\tau_{yz}\delta\gamma_{yz}]dAdz-\int_A q\delta w\ dA=0 \tag{12}$$

Where A is the surface in the top surface; q is the distributed transverse load.

Substituting Eqs. (8) and (10) into Eq. (12) and integrating through the thickness of the plate, we can obtain:

$$\begin{aligned}&\int_A[N_x\delta\varepsilon_x^0+M_x^b\delta k_x^b+M_x^s\delta k_x^s+N_y\delta\varepsilon_y^0+M_y^b\delta k_y^b+M_y^s\delta k_y^s+N_z\delta\varepsilon_z^0+N_{xy}\delta\gamma_{xy}^0+M_{xy}^b\delta k_{xy}^b\\ &+M_{xy}^s\delta k_{xy}^s+Q_{yz}^s\delta\gamma_{yz}^0+S_{yz}^s\delta\gamma_{yz}^0+Q_{xz}^s\delta\gamma_{xz}^0+S_{xz}^s\delta\gamma_{xz}^0]dA-\int_A q\delta w\ dA=0\end{aligned} \tag{13}$$

The stress resultants *N, M, Q,* and *S* are defined by:

$$\begin{Bmatrix}N_x & N_y & N_{xy}\\ M_x^b & M_y^b & M_{xy}^b\\ M_x^s & M_y^s & M_{xy}^s\end{Bmatrix}=\int_{-h/2}^{h/2}(\sigma_x,\sigma_y,\tau_{xy})\begin{Bmatrix}1\\ z\\ f(z)\end{Bmatrix}dz\ ,\ N_z=\int_{-h/2}^{h/2}\sigma_z\ \mathrm{g'(z)}\,dz$$
$$(S_{xz}^s,S_{yz}^s)=\int_{-h/2}^{h/2}(\tau_{xz},\tau_{yz})\ \mathrm{g(z)}\,dz\ ,\ (Q_{xz}^s,Q_{yz}^s)=\int_{-h/2}^{h/2}(\tau_{xz},\tau_{yz})\ f'(z)\,dz \tag{14}$$

The governing equations of equilibrium can be derived from eq. (13) by integrating the displacement gradients by parts and setting the coefficients where $\delta u_0,\delta v_0,\delta w_b,\delta w_s$ zero. Thus, one can obtain the equilibrium equations associated with the present shear deformation theory.

$$\begin{aligned}
&\delta u_0: && \frac{\partial N_x}{\partial x}+\frac{\partial N_{xy}}{\partial y}=0\\
&\delta v_0: && \frac{\partial N_{xy}}{\partial x}+\frac{\partial N_y}{\partial y}=0\\
&\delta w_b: && \frac{\partial^2 M_x^b}{\partial x^2}+2\frac{\partial^2 M_{xy}^b}{\partial x\partial y}+\frac{\partial^2 M_y^b}{\partial y^2}+q=0\\
&\delta w_s: && -\mathrm{N}_z-\frac{\partial^2 M_x^s}{\partial x^2}-\frac{\partial^2 M_x^s}{\partial y^2}-2\frac{\partial^2 M_{xy}^s}{\partial x\partial y}+\frac{\partial Q_{xz}^s}{\partial x}+\frac{\partial Q_{yz}^s}{\partial y}+\frac{\partial S_{xz}^s}{\partial x}+\frac{\partial S_{yz}^s}{\partial y}+qg(z)=0
\end{aligned} \tag{15}$$

The resulting constraints M, N, S, and Q can be written in matrix form as follows:

$$\begin{Bmatrix} N\\ M^b\\ M^s \end{Bmatrix}=\begin{bmatrix} A & B & B^s\\ B & D & D^s\\ B^s & D^s & H^s \end{bmatrix}\begin{Bmatrix} \varepsilon\\ k^b\\ k^s \end{Bmatrix}+\begin{bmatrix} L\\ L^a\\ R \end{bmatrix}\varepsilon_0^z \quad , \quad \begin{Bmatrix} Q\\ S \end{Bmatrix}=\begin{bmatrix} F^s & X^s\\ X^s & A^s \end{bmatrix}\begin{Bmatrix} \gamma^0\\ \gamma^1 \end{Bmatrix} \tag{16}$$
$$N_z=R^a\varepsilon_z^0+L(\varepsilon_x^0+\varepsilon_y^0)+L^a(k_x^b+k_y^b)+R(k_x^s+k_y^s)$$

$$\begin{aligned}
&N=\left\{N_x,N_y,N_{xy}\right\},\ M^b=\left\{M_x^b,M_y^b,M_{xy}^b\right\},\ M^s=\left\{M_x^s,M_y^s,M_{xy}^s\right\}\\
&S=\left\{S_{xz}^s,S_{yz}^s\right\},\ Q=\left\{Q_{xz}^s,Q_{yz}^s\right\}\\
&\gamma^0=\left\{\gamma_{xz}^0,\gamma_{yz}^0\right\},\ \gamma^1=\left\{\gamma_{xz}^1,\gamma_{yz}^1\right\}\\
&\varepsilon=\left\{\varepsilon_x^0,\varepsilon_y^0,\varepsilon_{xy}^0\right\},\ k^b=\left\{k_x^b,k_y^b,k_{xy}^b\right\},\ k^s=\left\{k_x^s,k_y^s,k_{xy}^s\right\}
\end{aligned} \tag{17}$$

$$\begin{aligned}
&A=\begin{bmatrix} A_{11} & A_{12} & 0\\ A_{12} & A_{22} & 0\\ 0 & 0 & A_{66} \end{bmatrix},\ B=\begin{bmatrix} B_{11} & B_{12} & 0\\ B_{12} & B_{22} & 0\\ 0 & 0 & B_{66} \end{bmatrix},\ D=\begin{bmatrix} D_{11} & D_{12} & 0\\ D_{12} & D_{22} & 0\\ 0 & 0 & D_{66} \end{bmatrix}\\
&B^s=\begin{bmatrix} B_{11}^s & B_{12}^s & 0\\ B_{12}^s & B_{22}^s & 0\\ 0 & 0 & B_{66}^s \end{bmatrix},\ \mathrm{D}^s=\begin{bmatrix} D_{11}^s & D_{12}^s & 0\\ D_{12}^s & D_{22}^s & 0\\ 0 & 0 & D_{66}^s \end{bmatrix},\ \mathrm{H}^s=\begin{bmatrix} H_{11}^s & H_{12}^s & 0\\ H_{12}^s & H_{22}^s & 0\\ 0 & 0 & H_{66}^s \end{bmatrix}
\end{aligned} \tag{18}$$

$$\begin{Bmatrix} L\\ L^a\\ R\\ R^a \end{Bmatrix}=\int_{-h/2}^{h/2} C_{ij}\begin{Bmatrix} 1\\ z\\ f(z)\\ g'(z)\dfrac{1-\nu}{\nu} \end{Bmatrix}g'(z)dz \tag{19}$$

Where the coefficients are determined by:

$$\begin{Bmatrix} A_{11} & B_{11} & D_{11} & B_{11}^s & D_{11}^s & H_{11}^s\\ A_{12} & B_{12} & D_{12} & B_{12}^s & D_{12}^s & H_{12}^s\\ A_{66} & B_{66} & D_{66} & B_{66}^s & D_{66}^s & H_{66}^s \end{Bmatrix}=\int_{-h/2}^{h/2}\left[1,\quad z,\quad z^2,\quad f(z),\quad zf(z),\quad f^2(z)\right]\begin{Bmatrix} C_{11}\\ C_{12}\\ C_{66} \end{Bmatrix}dz \tag{20}$$

$$F^s=\begin{bmatrix} F_{44}^s & 0\\ 0 & F_{55}^s \end{bmatrix},A^s=\begin{bmatrix} A_{44}^s & 0\\ 0 & A_{55}^s \end{bmatrix},X^s=\begin{bmatrix} X_{44}^s & 0\\ 0 & X_{55}^s \end{bmatrix} \tag{21}$$

$$(F_{44}^s, X_{44}^s, A_{44}^s) = (F_{55}^s, X_{55}^s, A_{55}^s) = \int_{-h/2}^{h/2} \left(\frac{E(z)}{2(1+\nu)}\right) [f'^2(z),\ f'(z)g(z),\ g^2(z)]\ dz \tag{22}$$

The governing equations of the theory used can be expressed in terms of displacements as follows:

$$\begin{aligned}\delta u_0: \quad & A_{11}\frac{\partial^2 u_0}{\partial x^2} + A_{12}\frac{\partial^2 v_0}{\partial x \partial y} + A_{66}\left(\frac{\partial^2 u_0}{\partial y^2} + \frac{\partial^2 v_0}{\partial x \partial y}\right) - B_{11}\frac{\partial^3 w_b}{\partial x^3} - B_{11}^s\frac{\partial^3 w_s}{\partial x^3} \\ & -(B_{12}+2B_{66})\frac{\partial^3 w_b}{\partial x \partial y^2} + L\frac{\partial w_s}{\partial x} + (B_{11}^s + 2B_{66}^s)\frac{\partial^3 w_s}{\partial x \partial y^2} = 0\end{aligned} \tag{23a}$$

$$\begin{aligned}\delta v_0: \quad & A_{22}\frac{\partial^2 v_0}{\partial y^2} + A_{66}\frac{\partial^2 v_0}{\partial x^2} + (A_{22}+A_{66})\frac{\partial^2 u_0}{\partial x \partial y} - B_{22}\frac{\partial^3 w_b}{\partial y^3} + B_{22}^s\frac{\partial^3 w_s}{\partial y^3} \\ & -(B_{12}+2B_{66})\frac{\partial^3 w_b}{\partial x^2 \partial y} + (B_{12}^s + 2B_{66}^s)\frac{\partial^3 w_s}{\partial x^2 \partial y} + L\frac{\partial w_s}{\partial y} = 0\end{aligned} \tag{23b}$$

$$\begin{aligned}\delta w_b: \quad & B_{11}\frac{\partial^3 u_0}{\partial x^3} + (B_{12}+2B_{66})\left(\frac{\partial^3 u_0}{\partial x \partial y^2} + \frac{\partial^3 v_0}{\partial x^2 \partial y}\right) + B_{22}\frac{\partial^3 v_0}{\partial y^3} - D_{11}\frac{\partial^4 w_b}{\partial x^4} \\ & -(2D_{12}+4D_{66})\frac{\partial^4 w_b}{\partial x^2 \partial y^2} - D_{22}\frac{\partial^4 w_b}{\partial y^4} + D_{11}^s\frac{\partial^4 w_s}{\partial x^4} + D_{22}^s\frac{\partial^4 w_s}{\partial y^4} \\ & +(D_{12}^s + 2D_{66}^s)\frac{\partial^4 w_s}{\partial x^2 \partial y^2} + q = 0\end{aligned} \tag{23c}$$

$$\begin{aligned}\delta w_s: \quad & -B_{11}^s\frac{\partial^3 u_0}{\partial x^3} - (B_{12}^s + 2B_{66}^s)\frac{\partial^3 u_0}{\partial x \partial y^2} - (B_{12}^s + 2B_{66}^s)\frac{\partial^3 v_0}{\partial x^2 \partial y} - B_{22}^s\frac{\partial^3 v_0}{\partial y^3} \\ & -L\frac{\partial u_0}{\partial x} - L\frac{\partial v_0}{\partial y} + D_{11}^s\frac{\partial^4 w_b}{\partial x^4} + D_{66}^s\frac{\partial^4 w_b}{\partial y^4} + 2(D_{12}^s + D_{66}^s)\frac{\partial^4 w_b}{\partial x^2 \partial y^2} \\ & +L^a\frac{\partial^2 w_b}{\partial x^2} + L^a\frac{\partial^2 w_b}{\partial y^2} - H_{11}^s\frac{\partial^4 w_s}{\partial x^4} - 2(H_{12}^s + H_{66}^s)\frac{\partial^4 w_s}{\partial x^2 \partial y^2} - H_{22}^s\frac{\partial^4 w_s}{\partial y^4} \\ & +(2F_{55}^s + X_{55}^s + A_{55}^s - 2R)\frac{\partial^2 w_s}{\partial x^2} + (2F_{44}^s + X_{44}^s + A_{44}^s - 2R)\frac{\partial^2 w_s}{\partial y^2} + qg(z) = 0\end{aligned} \tag{23d}$$

6. Solution approach

The boundary conditions along the edges of the simply supported plate can be obtained as:

$$\begin{aligned} & N_x = M_x^b = M_x^s = v = w_b = w_s = \frac{\partial w_s}{\partial y} \quad \text{at} \quad x=0,a \\ & N_y = M_y^b = M_y^s = u = w_b = w_s = \frac{\partial w_s}{\partial x} \quad \text{at} \quad y=0,b \end{aligned} \tag{24}$$

Using Navier's solution, solutions that meet the above boundary conditions can be written in the following form:

$$\begin{Bmatrix} u \\ v \\ w_b \\ w_s \end{Bmatrix} = \begin{Bmatrix} U\cos(\alpha x)\sin(\beta y) \\ V\sin(\alpha x)\cos(\beta y) \\ W_b\sin(\alpha x)\sin(\beta y) \\ W_s\sin(\alpha x)\sin(\beta y) \end{Bmatrix},\ q = q_0\sin(\alpha x)\sin(\beta y) \tag{26}$$

Where q_0 is constant, $\alpha = \pi/a$, $\beta = \pi/b$.

By substituting Eqs. (25) into Eqs. (24), the following equation are obtained:

$$[K]\{\Delta\} = \{Q\} \tag{26}$$

Where $\{\Delta\} = \{U, V, W_b, W_s\}^t$ and $\{Q\} = \{0, 0, -q_0, g(h/2)q_0\}^t$ is the symmetric matrix given by:

$$[K] = \begin{bmatrix} a_{11} & a_{12} & a_{13} & a_{14} \\ a_{12} & a_{22} & a_{23} & a_{24} \\ a_{13} & a_{23} & a_{33} & a_{34} \\ a_{14} & a_{24} & a_{34} & a_{44} \end{bmatrix} \tag{27}$$

In which:

$$\begin{aligned}
a_{11} &= (A_{11}\alpha^2 + A_{66}\beta^2) \\
a_{12} &= -\alpha\ \beta\ (A_{12} + A_{66}) \\
a_{13} &= \alpha(B_{11}\alpha^2 + (B_{12} + 2B_{66})\beta^2) \\
a_{14} &= -\alpha^3 B_{11}^s - (B_{12}^s + 2B_{66}^s)\alpha\beta^2 + L\alpha \\
a_{22} &= -(\alpha^2 A_{66} + \beta^2 A_{22}) \\
a_{23} &= \beta(B_{22}\beta^2 - (B_{12} + 2B_{66})\alpha^2) \\
a_{24} &= -\beta^3 B_{22}^s - (B_{12}^s + 2B_{66}^s)\alpha^2\beta + L\beta \\
a_{33} &= -\alpha^2\left(D_{11}\alpha^2 + \left(2D_{12} + 4D_{66}\right)\beta^2\right) - D_{22}\beta^4 \\
a_{34} &= \alpha^4 D_{11}^s + \beta^4 D_{22}^s + 2\alpha^2\beta^2(D_{12}^s + 2D_{66}^s) - L_a(\beta^2 + \alpha^2) \\
a_{44} &= -\alpha^4 H_{11}^s - \beta^4 H_{22}^s - 2\alpha^2\beta^2(H_{12}^s + 2H_{66}^s) - \beta^2(F_{44}^s + X_{44}^s) \\
&\quad -\alpha^2(F_{44}^s + X_{44}^s) - \beta^2(X_{44}^s + A_{44}^s) - \alpha^2(X_{44}^s + A_{44}^s) \\
&\quad + 2(\beta^2 + \alpha^2)R - R^a
\end{aligned} \tag{28}$$

7. Numerical results and discussion

In the present section, the effect of micromechanical models on bending analysis of FG plates using a new quasi-3D shear deformation theory is presented for investigation. In order to verify the accuracy of the present analysis, the results of this study were verified by comparing them with the various existing plate theories. The material properties used in the present study are:

- Ceramic (Pc: Alumina, Al2O3): Ec=380 GPa; υc=0.3.
- Metal (Pm: Aluminum, Al) : Em =70 GPa; υm=0.3.

The various non-dimensional parameters used in the present analysis are given below:

$$\bar{w} = \frac{10E_c h^3}{q_0 a^4} w\left(\frac{a}{2}, \frac{b}{2}\right),\ \bar{\sigma}_{xx}(z) = \frac{h}{q_0 a}\sigma_x\left(\frac{a}{2}, \frac{b}{2}, z\right),\ \bar{\sigma}_{yy}(z) = \frac{h}{q_0 a}\sigma_y\left(\frac{a}{2}, \frac{b}{2}, z\right),\ \bar{\tau}_{xz}(z) = \frac{h}{q_0 a}\tau_{xz}\left(0, \frac{b}{2}, z\right)$$

$$\bar{\tau}_{yz}(z) = \frac{h}{q_0 a}\tau_{yz}\left(\frac{a}{2}, 0, z\right), \bar{\tau}_{xy}(z) = \frac{h}{q_0 a}\tau_{xy}(0, 0, z)$$

Numerical results for the power-law FG plates k are presented in tables 1-2 using the present theory were compared with those of the classical plate theory [1] given by Timoshenko, the Navier-type three-dimensionally (3-D) exact solution given by Werner [33], the generalized shear deformation theory by Zenkour [20], and refined HSDT theory by Nguyen [34]. The present solution is appreciated for a quadratic plate, with the following fixed data: a = 1, b = 1, E = 1, q0 = 1, ν = 0.3 and three cases for the plate thickness: h = 0.01, h = 0.03, and h = 0.1.

It can be seen that is an excellent agreement between the obtained results in this paper and those reported in [1, 20, 34]. It can be observed that in the mid-plane for the case of the isotropic plate the axial stress equaled zero. Therefore, the neutral surface was identical to mid-plane for the isotropic plate.

Table 1: Comparison of center deflections of the isotropic homogeneous plates.

h	Classical [1]	3-D [1]	SSDT [20]	Nguyen et al [1]	Present
0.01	44360.9	44384.7	44383.84	44385.41	44379.49
0.03	1643.00	1650.94	1650.646	1651.169	1649.247
0.1	44.3609	46.7443	46.65481	46.81271	46.29049

Table 2 : Comparison of distribution of stress across the depth of isotropic homogeneous plates.

h	z/h	σ_{xx}				τ_{xy}			
		3-D [1]	SSDT [20]	Nguyen et al [1]	Present	3-D [1]	SSDT [20]	Nguyen et al [1]	Present
0.01	0.5	2873.3	2873.39	2873.51	2873.74	1949.6	1949.36	1948.61	1947.86
	0.4	2298.6	2298.57	2298.86	2298.78	1559.2	1559.04	1558.85	1556.68
	0.3	1723.9	1723.84	1724.22	1725.70	1169.1	1168.99	1169.09	1168.26
	0.2	1149.2	1149.18	1149.58	1149.26	779.3	779.18	779.33	778.35
	0.1	574.6	574.58	574.93	574.61	389.6	389.55	389.56	389.13
	0.0	0.00	0.00	0.00	0.00	0.00	0.00	0.00	0.00
0.03	0.5	319.40	319.445	319.279	319.825	217.11	217.156	216.512	216.046
	0.4	255.41	255.415	255.429	255.658	173.26	173.282	173.205	172.378
	0.3	191.49	191.472	191.580	191.817	129.75	129.682	129.897	129.129
	0.2	127.63	127.603	127.731	127.693	86.41	86.313	86.592	85.852
	0.1	63.80	63.788	63.881	63.830	43.18	43.112	43.285	42.946
	0.0	0.00	0.00	0.00	0.00	0.00	0.00	0.00	0.00
0.1	0.5	28.890	28.9307	28.7351	29.2565	19.920	20.0476	19.4861	19.5282
	0.4	22.998	23.0055	22.9887	23.2120	15.606	15.6459	15.5885	15.2717
	0.3	17.182	17.1660	17.2422	17.3135	11.558	11.4859	11.6909	11.2408
	0.2	11.423	11.3994	11.4958	11.4769	7.642	7.5315	7.7933	7.4055
	0.1	5.702	5.6858	5.7493	5.7223	3.803	3.7265	3.8957	3.6631
	0.0	0.00	0.00	0.00	0.00	0.00	0.00	0.00	0.00

Materials properties are defined by using the power-law distribution. The results obtained are compared with those obtained by Zenkour [9] using the sinusoidal shear deformation plate theory SSDT and the higher order shear deformation plate theory using by Nguyen [35] with different value of power law index k and aspect ratio a/h = 10.

From tables 3 and 4, it can be seen that is an excellent agreement between the obtained results in this paper and those reported in [9, 35].

Table 3 : Non-dimensional displacements and stress of an FGM square plate under uniform load (a/h = 10).

k	Theory	w	$\bar{\sigma}_{xx}$	$\bar{\sigma}_{yy}$	$\bar{\tau}_{yz}$	$\bar{\tau}_{xz}$	$\bar{\tau}_{yz}$
0	Present	0.46288	2.9254	1.9253	0.48704	0.54794	1.2563
	SSDT [20]	0.4665	2.8932	1.9103	0.4429	0.5114	1.2850
	Nguyen et al [35]	0.4681	2.8732	1.9155	0.4665	0.5386	1.2993
1	Present	0.89688	4.4879	2.1292	0.5990	0.5481	1.0167
	SSDT [20]	0.9287	4.4745	2.1692	0.5446	0.5114	1.1143
	Nguyen et al [35]	0.9262	4.4408	2.1768	0.5010	0.4705	1.1221
2	Present	1.1391	5.2170	1.9677	0.56342	0.44998	0.89686
	SSDT [20]	1.1940	5.2296	2.0338	0.5734	0.4700	0.9907
	Nguyen et al [35]	1.1863	5.1853	2.0442	0.4757	0.3899	1.0000

	Present	1.3733	6.0480	1.5353	0.40911	0.33095	0.96196
5	SSDT [20]	1.4356	6.1504	1.6104	0.5031	0.4177	1.0451
	Nguyen et al [35]	1.4211	6.0858	1.6253	0.4014	0.3333	1.0593
	Present	1.5402	7.2262	1.2323	0.34027	0.35724	1.0053
10	SSDT [20]	1.5876	7.3689	1.2820	0.4227	0.4552	1.0694
	Nguyen et al [35]	1.5841	7.2965	1.2954	0.3900	0.4200	1.0855
	Present	2.5131	2.9254	1.9255	0.48710	0.54819	1.2578
∞	SSDT [20]	2.5327	2.8932	1.9103	0.4429	0.5114	1.2850
	Nguyen et al [35]	2.5413	2.8732	1.9155	0.4665	0.5386	1.2993

Table 4 : Non-dimensional displacements and stress of an FGM square plate under sinusoidal load (a/h = 10).

k	Theory	w	$\bar{\sigma}_{xx}$	$\bar{\sigma}_{yy}$	$\bar{\tau}_{yz}$	$\bar{\tau}_{xz}$	$\bar{\tau}_{yz}$
	Present	0.2935	2.0211	1.3240	0.2428	0.2731	0.6932
0	SSDT [20]	0.2960	1.9955	1.3121	0.2132	0.2462	0.7065
	Nguyen et al [35]	0.2971	1.9758	1.3172	0.2205	0.2546	0.7092
	Present	0.5684	3.1022	1.4648	0.2985	0.2731	0.5618
1	SSDT [20]	0.5889	3.0870	1.4894	0.2622	0.2462	0.6110
	Nguyen et al [35]	0.5872	3.0537	1.4969	0.2369	0.2224	0.6125
	Present	0.7223	3.6031	1.3507	0.2757	0.2202	0.4943
2	SSDT [20]	0.7573	3.6094	1.3954	0.2763	0.2265	0.5441
	Nguyen et al [35]	0.7520	3.5657	1.4057	0.2249	0.1843	0.5459
	Present	0.8721	4.1765	1.0510	0.1940	0.1569	0.5291
5	SSDT [20]	0.9118	4.2488	1.1029	0.2429	0.2017	0.5755
	Nguyen et al [35]	0.9018	4.1849	1.1176	0.1898	0.1576	0.5783
	Present	0.9785	4.9911	0.8429	0.1610	0.1689	0.5537
10	SSDT [20]	1.0089	5.0890	0.8775	0.2041	0.2198	0.5894
	Nguyen et al [35]	1.0065	5.0175	0.8908	0.1844	0.1986	0.5926
	Present	1.5938	2.0210	1.3240	0.2428	0.2731	0.6933
∞	SSDT [20]	1.6070	1.9955	1.3172	0.2132	0.2462	0.7065
	Nguyen et al [35]	1.6129	1.9758	1.3121	0.2205	0.2546	0.7092

Table 5 displays the effects of geometrical ratio a/b on the dimensionless centre deflection of exponential model FGM rectangular plates with various power law index k for different value of the aspect ratio a/h. The acquired are compared with those of the 3D elasticity solution [36], quasi-3D theories [36, 37].

The correctness of the results is shown by the comparison of the results with the results for medium thick plates. It is observed that the deflections obtained of the proposed theory were a little larger than those of literature results for the very thick FGM plates (a/h = 2), because the effect of stretching did not take for the present theory.

Table 5 : Dimensionless center deflection ($\bar{W}$) of exponential model FGM rectangular plates.

a/h	b/a	Theory	k					
			0.1	0.3	0.5	0.7	1	1.5
		3D [36]	0.5769	0.5247	0.4766	0.4324	0.3727	0.2890
	1	Quasi-3D [36]	0.5731	0.5181	0.4679	0.4222	0.3612	0.2771
		Quasi-3D [37]	0.5776	0.5222	0.4716	0.4255	0.3640	0.2792
2		Present	0.5524	0.5420	0.4890	0.4411	0.3767	0.2879
		3D [36]	1.1944	1.0859	0.9864	0.8952	0.7727	0.6017
	2	Quasi-3D [36]	1.1880	1.0740	0.9701	0.8755	0.7494	0.5758
		Quasi-3D [37]	1.1938	1.0790	0.9748	0.8797	0.7530	0.5785

		Present	1.1665	1.0993	0.9927	0.8955	0.7658	0.5872
	3	3D [36]	1.4430	1.3116	1.1913	1.0812	0.9334	0.7275
		Quasi-3D [36]	1.4354	1.2977	1.1722	1.0580	0.9057	0.6962
		Quasi-3D [37]	1.4419	1.3035	1.1774	1.0626	0.9096	0.6991
		Present	1.4147	1.3234	1.1952	1.0783	0.92250	0.7078
4	1	3D [36]	0.3490	0.3168	0.2875	0.2608	0.2253	0.1805
		Quasi-3D [36]	0.3475	0.3142	0.2839	0.2563	0.2196	0.1692
		Quasi-3D [37]	0.3486	0.3152	0.2848	0.2571	0.2203	0.1697
		Present	0.3456	0.3159	0.2854	0.2577	0.2209	0.1702
	2	3D [36]	0.8153	0.7395	0.6708	0.6085	0.5257	0.4120
		Quasi-3D [36]	0.8120	0.7343	0.6635	0.5992	0.5136	0.3962
		Quasi-3D [37]	0.8145	0.7365	0.6655	0.6009	0.5151	0.3973
		Present	0.8098	0.73578	0.66500	0.6007	0.5151	0.3976
	3	3D [36]	1.0134	0.9190	0.8335	0.7561	0.6533	0.5121
		Quasi-3D [36]	1.0094	0.9127	0.8248	0.7449	0.6385	0.4927
		Quasi-3D [37]	1.0124	0.9155	0.8272	0.7470	0.6404	0.4941
		Present	1.0071	0.9142	0.8263	0.7464	0.6402	0.4943

Table 6 demonstrates comparison of dimensionless stress ($\bar{\sigma}_{xx}$) of exponential model FGM square plates with exponential material law for various values of *a/h*. The results of present theory are compared with the Arani and Zamani [38], the quasi-3D solutions of Mantari and Soares [39], and quasi-3D sinusoidal solution of Thai and Kim [40]. The numerical results indicate good agreement with corresponding literatures.

Table 6 : Dimensionless stress ($\bar{\sigma}_{xx}$) of exponential model FGM square plates.

a/h	Theory	k		
		0.7	1	1.5
2	HSDT [9] ($\varepsilon_z = 0$)	0.3123	0.3477	0.4035
	Arani and Zamani [38] ($\varepsilon_z \neq 0$)	0.3572	0.4045	0.4830
	Quasi-3D [40] ($\varepsilon_z \neq 0$)	0.3675	0.4085	0.4851
	Present ($\varepsilon_z \neq 0$)	0.3232	0.3574	0.4220
4	HSDT [9] ($\varepsilon_z = 0$)	0.2649	0.2927	0.3451
	Arani and Zamani [38] ($\varepsilon_z \neq 0$)	0.2822	0.3252	0.3722
	Quasi-3D [40] ($\varepsilon_z \neq 0$)	0.2870	0.3171	0.3739
	Present ($\varepsilon_z \neq 0$)	0.2712	0.2987	0.3506
10	HSDT [9] ($\varepsilon_z = 0$)	0.2515	0.2774	0.3264
	Arani and Zamani [38] ($\varepsilon_z \neq 0$)	0.2636	0.2902	0.3451
	Quasi-3D [40] ($\varepsilon_z \neq 0$)	0.2671	0.2944	0.3460
	Present ($\varepsilon_z \neq 0$)	0.2529	0.2781	0.3267

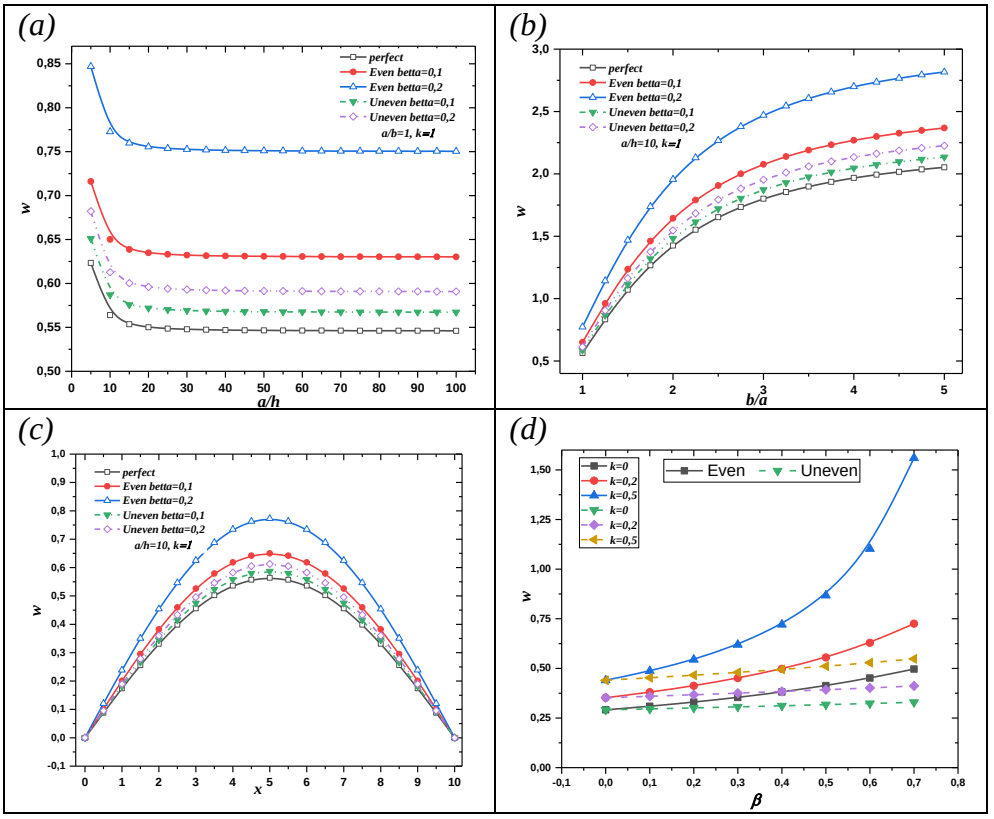

Fig 3 : Variation of the non-dimensional center deflection according to the parameter's a/h, b/a, x, beta in the case of porous P-FGM plates.

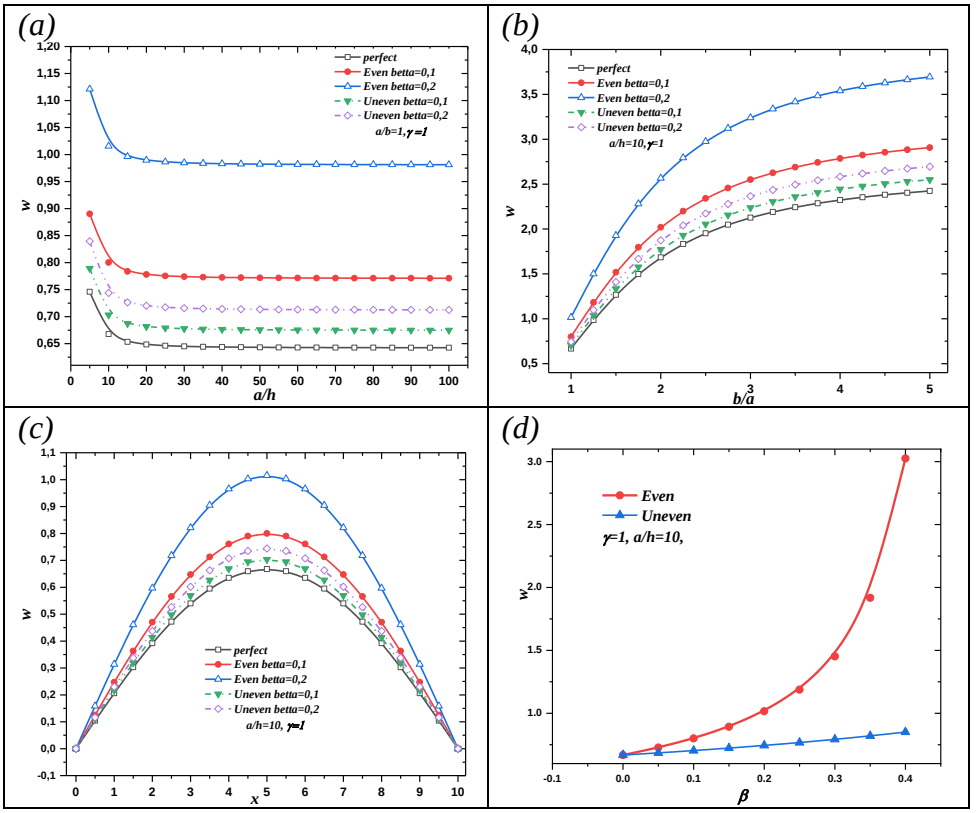

Fig 4 : Variation of the non-dimensional centre deflection according to the parameter's a/h, b/a, x, beta in the case of E-FGM plates.

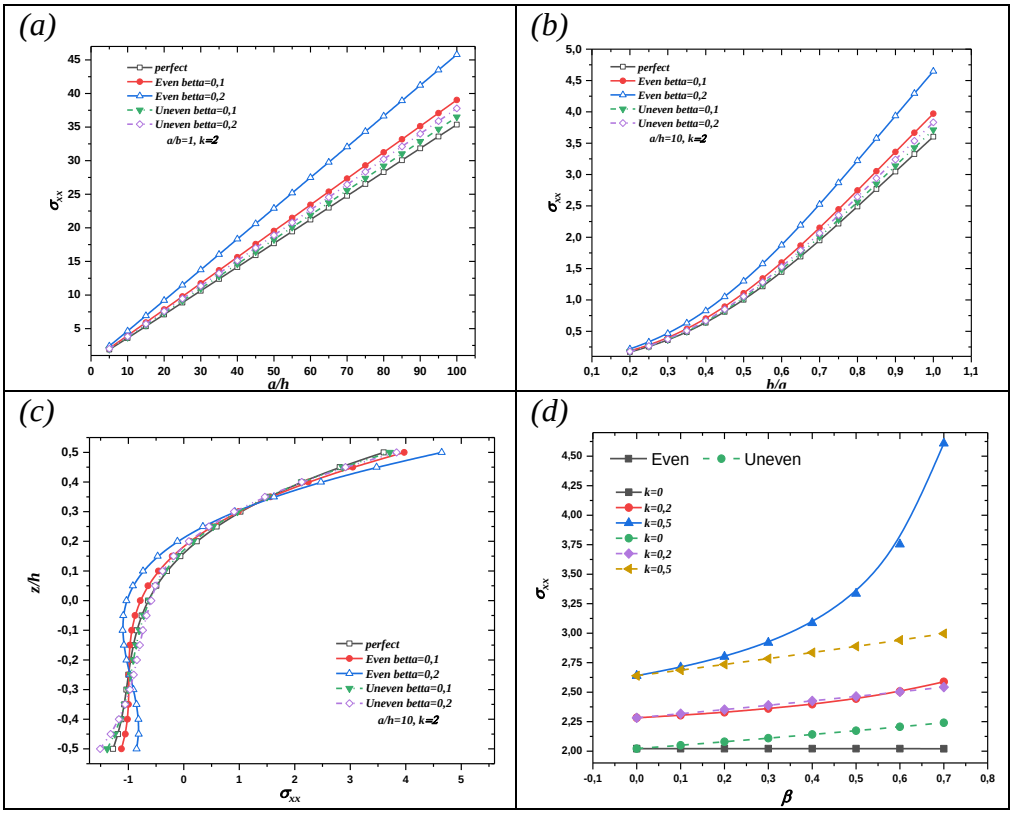

Fig 5 : Variation of the non-dimensional axial stress according to the parameter's a/h, b/a, x, beta in the case of P-FGM plates.

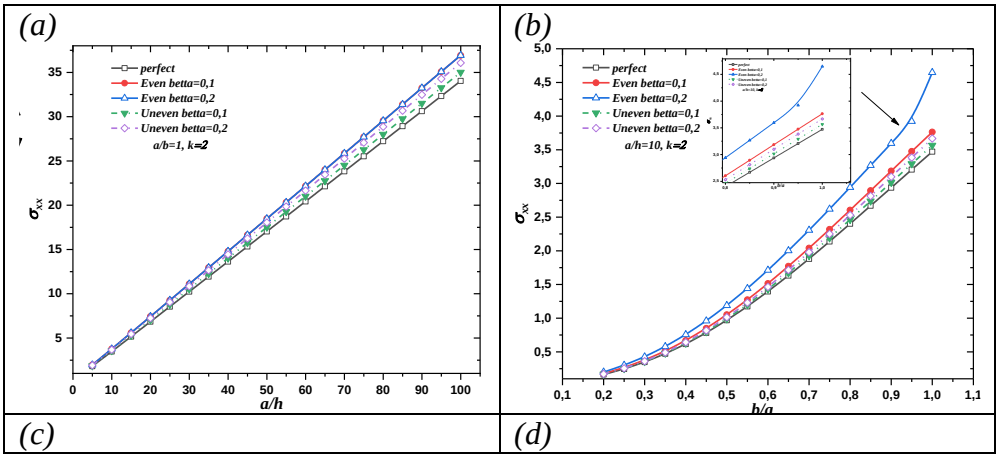

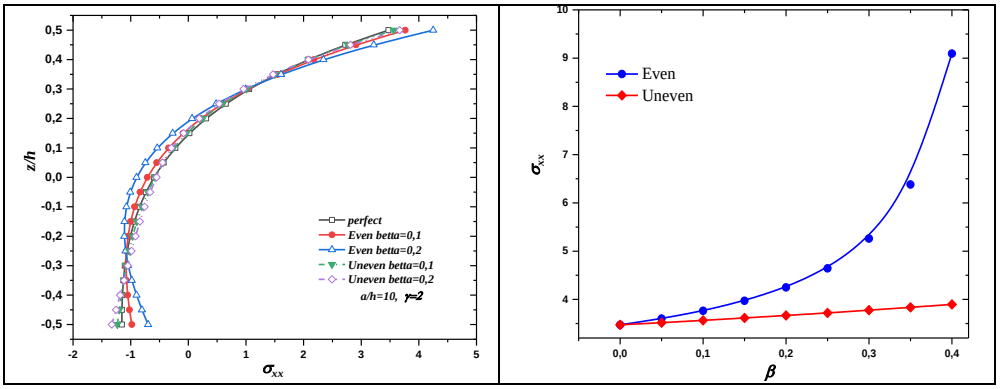

Fig 6 : Variation of the non-dimensional center axial stress according to the parameter's a/h, b/a, x, beta in the case of E-FGM plates.

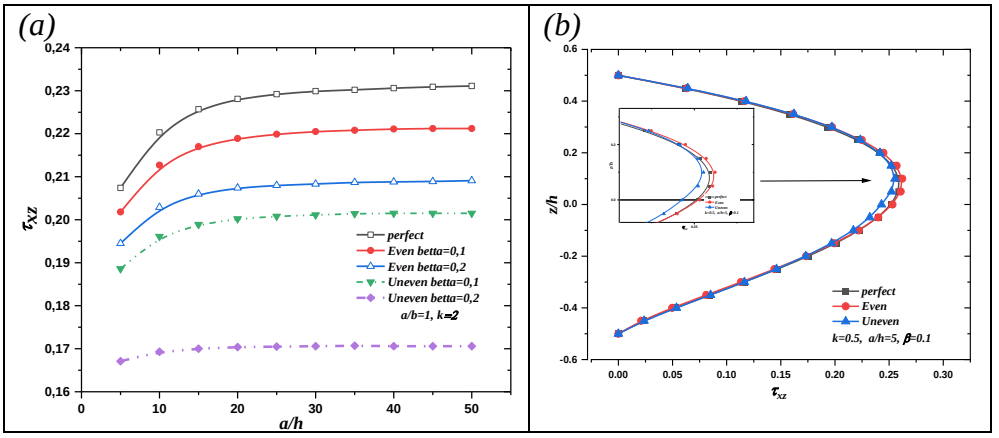

Fig 7 : Variation of the non-dimensional shear stress according to the parameter's a/h, b/a, x, beta in the case of P-FGM plates.

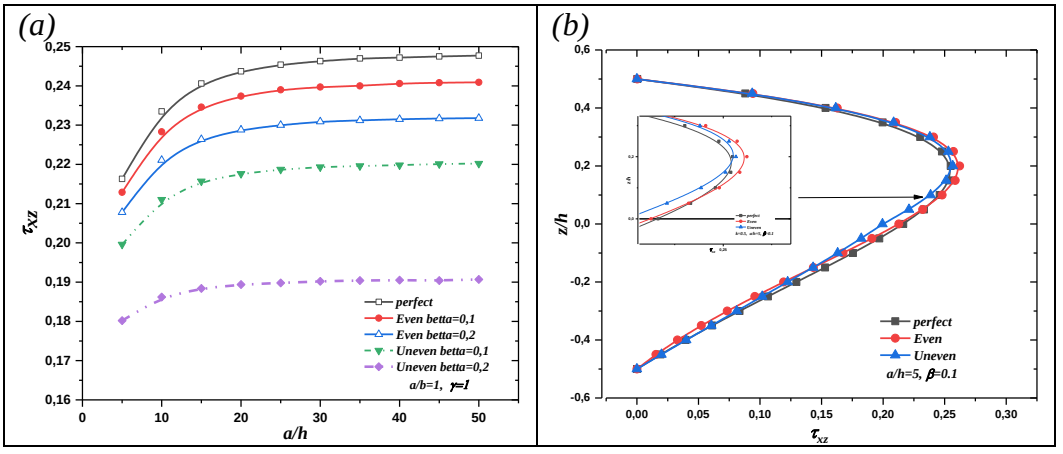

Fig 8 : Variation of the non-dimensional shear stress according to the parameter's a/h, b/a, x, beta in the case of S-FGM plates.

A comparison study of the center deflection and stress σxx are reported in figures 3-6 for P-FGM and E-FGM FG plates with various porous models. Figures 3a-6a indicate the effect of the side-to-thickness ratio a/h and the porosity models on the center deflections w (Figs. 3a-4a) and the dimensionless stress σxx (Figs. 5a-6a) of FG square plates with volume fraction k=1 and porosity coefficient β is chosen as 0.1 and 0.2. It is noted that the difference between perfect and imperfect porous models of P-FGM and E-FGM plates witch the center deflections w and the dimensionless stress σxx decreases with increasing of side-to-thickness ratio this is because of the porosity coefficient's effect on the plate's stiffness.

. It's seen in Figures 3b-6b the effect the aspect ratio b/a and the porosity models on the center deflections w (Figs. 3b-6b) and the dimensionless stress σxx (Figs. 5b-6b) of FG plates with volume fraction *k*=1, the side-to-thickness ratio a/h=10 and porosity coefficient β is chosen as 0.1 and 0,2. It is observed for both models of P-FGM and E-FGM plates that for perfect and imperfect porous, the deflection and stress increase rapidly with increasing of aspect ratio. It is clear that the central deflections w and the dimensionless stress σxx for FG plate with even porosity distribution model (β=0.2) are higher than for the other distribution models of P-FGM and E-FGM plates, because even porosity implies a uniform distribution of pores throughout the plate. This creates a more homogeneous material structure, meaning the material behaves similarly across different regions. This homogeneity leads to more efficient load transfer and reduced stress concentrations, resulting in higher stiffness and resistance to deformation.

Figures 3c and 4c demonstrate the center deflections w of P-FGM and E-FGM plates plots, using perfect and imperfect porous models. It can be seen that the center deflections w has maximum values at the center of the plate (x = a/2) significant differences between the results obtained by the porosity distribution models, where the even porosity distribution model (β=0.2) is higher than that for the other models.

Variation of porosity coefficient on the central deflection and stress for different volume fraction k of P-FGM and E-FGM plate are illustrated in figures 3d and 5d, respectively. The porosity coefficient β has an important effect on the deflections and stress mainly for all distribution models where the increasing of porosity coefficient increases the central deflections w and the stress σxx. Also, it is found that for figures 4d and 6d, where the central deflection and stress have important values for even porosity distribution model than uneven porosity distribution model of E-FGM plate, due to an increased porosity coefficient in an FG plate compromises its stiffness and increases stress concentration, leading to larger central deflections and higher overall stress under load.

The curves presented in figures 5c and 6c indicate the evolution of the normal stress σxx as a function of the z/h ratio and the porosity distribution for P-FGM and E-FGM plates. These curves indicate that the effect of the porosity parameter on normal stress σxx behaviour is the same as that observed for deflection, that is to say that the rise of the porosity parameter β leads to an increase of the normal stress σxx and this for the two types of FGM. The highest positive normal stress σxx value is obtained for non-uniform porosity distribution with β =0.1, whereas the smallest is obtained for non-uniform porosity repartition with β =0.2. The other values of normal stress σxx for the different cases are in this interval. It should also be noted that the values obtained in the case of P-FGM plates are inferior by a value almost equal to 50% of those obtained in the case of E-FGM, because the steeper stiffness gradient in E-FGM leads to a more efficient distribution of material properties compared to P-FGM under various loading conditions (bending, deflection, etc.).

Figures 7a-7b and 8a-8b show the transverse shear stresses τxz shape according to the variation of thickness ratio z/h and aspect ratio a/h. It's obvious that both of functionally graded porous and nonporous plates have the same behaviour. The shear stresses τxz maximum value given by the figures 7a-7b and 8a-8b are those obtained by the perfect functionally graded plate and the lowest by the uneven porosity distribution with β =0.2. However, it was also noted that the stresses obtained by the even distribution of the porosity are greater than those obtained by the uneven distribution, it means that, the uneven porosity distribution creates variations in material density across the plate's thickness. This can affect the stress distribution and potentially lead to higher shear stresses in specific regions compared to even porosity. The transverse shear stresses are affected by the variation of a/h ratio, the increase of this ratio has the effect of increasing the value of the stress, nevertheless this value has tendency to stabilize from a ratio a/h =30.

After reviewing the various results and interpretation of the different curves of the deflection, normal and shear stresses given established during this analysis, it can be concluded that the plates with the model P-FGM and E-FGM present the same behaviour and this even after introduction of the porosity effect. Nevertheless, the values of deflection, normal and shear stresses reached for E-FGM plates are greater than those of P-FGM plates.

8. Conclusions

This investigation explores the influence of porosity model distribution on the behavior of functionally graded plates using an innovative quasi-3D refined higher-order shear deformation theory. Unlike other quasi-3D theories with five or more unknowns, this work employs a displacement field limited to four unknowns. Additionally, it reduces the number of equilibrium equations, seamlessly integrating thickness-stretching effects into transverse displacement, bending, and shear. The study includes a comparison between two functionally graded material

models, namely P-FGM and E-FGM. The governing equations are derived from the static version of the principle of virtual work, and analytical solutions for simply supported P-FGM, E-FGM porous, and perfect plates are obtained. Multiple validation examples are presented and the current quasi-30 theory's numerical results accurately predict the bending response different FG plates. The same comportment is observed for plates with and without porosity, however an increase is observed in the values of deflection, normal and shear stresses in the case where the porosity is taken into account. In addition, the results obtained in terms of values of deflection, normal and shear stresses are higher in the case of E-FGM compared to P-FGM.[41, 42]

References

[1] M. Dhuria, N. Grover, K. Goyal, Influence of porosity distribution on static and buckling responses of porous functionally graded plates, in *Proceeding of,* Elsevier, pp. 1458-1474.

[2] A. Bouhadra, A. Menasria, M. A. Rachedi, Boundary conditions effect for buckling analysis of porous functionally graded nanobeam, *Advances in nano research,* Vol. 10, No. 4, pp. 313-325, 2021.

[3] E. Reissner, Y. Stavsky, Bending and stretching of certain types of heterogeneous aeolotropic elastic plates, 1961.

[4] E. Arshid, A. R. Khorshidvand, Free vibration analysis of saturated porous FG circular plates integrated with piezoelectric actuators via differential quadrature method, *Thin-Walled Structures,* Vol. 125, pp. 220-233, 2018.

[5] L. Della Croce, P. Venini, Finite elements for functionally graded Reissner–Mindlin plates, *Computer Methods in Applied Mechanics and Engineering,* Vol. 193, No. 9-11, pp. 705-725, 2004.

[6] S. Trabelsi, A. Frikha, S. Zghal, F. Dammak, Thermal post-buckling analysis of functionally graded material structures using a modified FSDT, *International Journal of Mechanical Sciences,* Vol. 144, pp. 74-89, 2018.

[7] E. Carrera, Theories and finite elements for multilayered, anisotropic, composite plates and shells, *Archives of computational methods in engineering,* Vol. 9, pp. 87-140, 2002.

[8] E. Carrera, G. Giunta, P. Nali, M. Petrolo, Refined beam elements with arbitrary cross-section geometries, *Computers & structures,* Vol. 88, No. 5-6, pp. 283-293, 2010.

[9] M. Arefi, M. Kiani, A. M. Zenkour, Size-dependent free vibration analysis of a three-layered exponentially graded nano-/micro-plate with piezomagnetic face sheets resting on Pasternak's foundation via MCST, *Journal of Sandwich Structures & Materials,* Vol. 22, No. 1, pp. 55-86, 2020.

[10] W.-Y. Jung, W.-T. Park, S.-C. Han, Bending and vibration analysis of S-FGM microplates embedded in Pasternak elastic medium using the modified couple stress theory, *International Journal of Mechanical Sciences,* Vol. 87, pp. 150-162, 2014.

[11] A. Tounsi, A. Bouhadra, A. A. Bousahla, S. Mahmoud, A new and simple HSDT for thermal stability analysis of FG sandwich plates, *Steel and Composite Structures, An International Journal,* Vol. 25, No. 2, pp. 157-175, 2017.

[12] M. Mohamed, T. Abdelouahed, M. Slimane, A refined of trigonometric shear deformation plate theory based on neutral surface position is proposed for static analysis of FGM plate, *Procedia Structural Integrity,* Vol. 26, pp. 129-138, 2020.

[13] S. R. Bathini, A refined inverse hyperbolic shear deformation theory for bending analysis of functionally graded porous plates, *Journal of Computational Applied Mechanics,* Vol. 51, No. 2, pp. 417-431, 2020.

[14] A. Benachour, H. D. Tahar, H. A. Atmane, A. Tounsi, M. S. Ahmed, A four variable refined plate theory for free vibrations of functionally graded plates with arbitrary gradient, *Composites Part B: Engineering,* Vol. 42, No. 6, pp. 1386-1394, 2011.

[15] V. T. Do, V. V. Pham, H. N. Nguyen, On the development of refined plate theory for static bending behavior of functionally graded plates, *Mathematical Problems in Engineering,* Vol. 2020, pp. 1-13, 2020.

[16] R. B. Bouiadjra, A. Mahmoudi, S. Benyoucef, A. Tounsi, F. Bernard, Analytical investigation of bending response of FGM plate using a new quasi 3D shear deformation theory: Effect of the micromechanical models, *Structural Engineering and Mechanics, An Int'l Journal,* Vol. 66, No. 3, pp. 317-328, 2018.

[17] M. Bennoun, M. S. A. Houari, A. Tounsi, A novel five-variable refined plate theory for vibration analysis of functionally graded sandwich plates, *Mechanics of Advanced Materials and Structures,* Vol. 23, No. 4, pp. 423-431, 2016.

[18] H. Bellifa, A. Bakora, A. Tounsi, A. A. Bousahla, S. R. Mahmoud, An efficient and simple four variable refined plate theory for buckling analysis of functionally graded plates, *Steel and Composite Structures, An International Journal,* Vol. 25, No. 3, pp. 257-270, 2017.

[19] F. Z. Taibi, S. Benyoucef, A. Tounsi, R. Bachir Bouiadjra, E. A. Adda Bedia, S. Mahmoud, A simple shear deformation theory for thermo-mechanical behaviour of functionally graded sandwich plates on elastic foundations, *Journal of Sandwich Structures & Materials,* Vol. 17, No. 2, pp. 99-129, 2015.

[20] A. M. Zenkour, Generalized shear deformation theory for bending analysis of functionally graded plates, *Applied Mathematical Modelling,* Vol. 30, No. 1, pp. 67-84, 2006.

[21] M. Bouazza, A. Boucheta, T. Becheri, N. Benseddiq, Thermal stability analysis of functionally graded plates using simple refined plate theory, *International Journal of Automotive and Mechanical Engineering,* Vol. 14, pp. 4013-4029, 2017.

[22] S. Merdaci, H. Belghoul, High-order shear theory for static analysis of functionally graded plates with porosities, *Comptes Rendus Mécanique,* Vol. 347, No. 3, pp. 207-217, 2019/03/01/, 2019.

[23] A. R. Khorshidvand, A. R. Damercheloo, Bending, axial buckling and shear buckling analyses of FG-porous plates based on a refined plate theory, *Australian Journal of Mechanical Engineering,* Vol. 21, No. 2, pp. 705-724, 2023.

[24] A. B. Rad, Static analysis of non-uniform 2D functionally graded auxetic-porous circular plates interacting with the gradient elastic foundations involving friction force, *Aerospace Science and Technology,* Vol. 76, pp. 315-339, 2018.

[25] I. J. Maknun, S. Natarajan, I. Katili, Application of discrete shear quadrilateral element for static bending, free vibration and buckling analysis of functionally graded material plate, *Composite Structures,* Vol. 284, pp. 115130, 2022.

[26] S. K. Sah, A. Ghosh, Influence of porosity distribution on free vibration and buckling analysis of multi-directional functionally graded sandwich plates, *Composite Structures,* Vol. 279, pp. 114795, 2022.

[27] L. T. Hai, N. Van Long, T. M. Tu, C. T. Binh, Post-buckling response of functionally graded porous plates rested on elastic substrate via first-order shear deformation theory, in *Proceeding of,* Springer, pp. 761-779.

[28] F. Abdoun, L. Azrar, Nonlinear thermal analysis of multilayered composite and FGM plates with temperature-dependent properties based on an asymptotic numerical method, *Archive of Applied Mechanics,* Vol. 91, No. 10, pp. 4361-4387, 2021.

[29] M. Di Sciuva, M. Sorrenti, Bending, free vibration and buckling of functionally graded carbon nanotube-reinforced sandwich plates, using the extended Refined Zigzag Theory, *Composite Structures,* Vol. 227, pp. 111324, 2019.

[30] M. W. Zaitoun, A. Chikh, A. Tounsi, M. A. Al-Osta, A. Sharif, S. U. Al-Dulaijan, M. M. Al-Zahrani, Influence of the visco-Pasternak foundation parameters on the buckling behavior of a sandwich functional graded ceramic–metal plate in a hygrothermal environment, *Thin-Walled Structures,* Vol. 170, pp. 108549, 2022.

[31] A. Bakoura, F. Bourada, A. A. Bousahla, A. Tounsi, K. H. Benrahou, A. Tounsi, M. M. Al-Zahrani, S. Mahmoud, Buckling analysis of functionally graded plates using HSDT in conjunction with the stress function method, *Computers and Concrete, An International Journal,* Vol. 27, No. 1, pp. 73-83, 2021.

[32] S. Refrafi, A. A. Bousahla, A. Bouhadra, A. Menasria, F. Bourada, A. Tounsi, E. A. Bedia, S. Mahmoud, K. H. Benrahou, A. Tounsi, Effects of hygro-thermo-mechanical conditions on the buckling of FG sandwich plates resting on elastic foundations, *Computers and Concrete, an International Journal,* Vol. 25, No. 4, pp. 311-325, 2020.

[33] H. Werner, A three-dimensional solution for rectangular plate bending free of transversal normal stresses, *Communications in numerical methods in engineering,* Vol. 15, No. 4, pp. 295-302, 1999.

[34] F. Y. Genao, J. Kim, K. K. Żur, Nonlinear finite element analysis of temperature-dependent functionally graded porous micro-plates under thermal and mechanical loads, *Composite Structures,* Vol. 256, pp. 112931, 2021.

[35] N. V. Nguyen, L. B. Nguyen, H. Nguyen-Xuan, J. Lee, Analysis and active control of geometrically nonlinear responses of smart FG porous plates with graphene nanoplatelets reinforcement based on Bézier extraction of NURBS, *International Journal of Mechanical Sciences,* Vol. 180, pp. 105692, 2020.

[36] A. Zenkour, Benchmark trigonometric and 3-D elasticity solutions for an exponentially graded thick rectangular plate, *Archive of Applied Mechanics,* Vol. 77, No. 4, pp. 197-214, 2007.

[37] J. Mantari, C. G. Soares, Generalized hybrid quasi-3D shear deformation theory for the static analysis of advanced composite plates, *Composite Structures,* Vol. 94, No. 8, pp. 2561-2575, 2012.

[38] A. Ghorbanpour Arani, M. Zamani, Investigation of electric field effect on size-dependent bending analysis of functionally graded porous shear and normal deformable sandwich nanoplate on silica Aerogel foundation, *Journal of Sandwich Structures & Materials,* Vol. 21, No. 8, pp. 2700-2734, 2019.

[39] J. Mantari, C. G. Soares, A novel higher-order shear deformation theory with stretching effect for functionally graded plates, *Composites Part B: Engineering,* Vol. 45, No. 1, pp. 268-281, 2013.

[40] H.-T. Thai, S.-E. Kim, A simple higher-order shear deformation theory for bending and free vibration analysis of functionally graded plates, *Composite Structures,* Vol. 96, pp. 165-173, 2013.

[41] M. Al-Furjan, M. Xu, A. Farrokhian, G. S. Jafari, X. Shen, R. Kolahchi, On wave propagation in piezoelectric-auxetic honeycomb-2D-FGM micro-sandwich beams based on modified couple stress and refined zigzag theories, *Waves in Random and Complex Media*, pp. 1-25, 2022.

[42] M. Al-Furjan, S. Fan, L. Shan, A. Farrokhian, X. Shen, R. Kolahchi, Wave propagation analysis of micro air vehicle wings with honeycomb core covered by porous FGM and nanocomposite magnetostrictive layers, *Waves in Random and Complex Media*, pp. 1-30, 2023.